MATHEMATICAL ENGINEERING
TECHNICAL REPORTS

A Mixed Integer Programming Approach to Designing Periodic Frame Structures with Negative Poisson's Ratio

Rui KURETA and Yoshihiro KANNO

METR 2012–16 October 2012

DEPARTMENT OF MATHEMATICAL INFORMATICS
GRADUATE SCHOOL OF INFORMATION SCIENCE AND TECHNOLOGY
THE UNIVERSITY OF TOKYO
BUNKYO-KU, TOKYO 113-8656, JAPAN

WWW page: http://www.keisu.t.u-tokyo.ac.jp/research/techrep/index.html

A Mixed Integer Programming Approach to Designing Periodic Frame Structures with Negative Poisson's Ratio

Rui Kureta [†], Yoshihiro Kanno [‡]

Department of Mathematical Informatics,
University of Tokyo, Tokyo 113-8656, Japan

Abstract

Materials and microstructures with specific configurations are able to have negative Poisson's ratio. This paper proposes a topology optimization methodology of frame structures to design a planar periodic structure that exhibits negative Poisson's ratio. Provided that beam section of each existing member is chosen from a set of some given candidates, the topology optimization problem can be reduced to a mixed integer linear programming (MILP) problem. Since the proposed approach treats frame structures and stress constraints are rigorously addressed, no link-mechanism is generated. A heuristic method with local search is used to solve large-scale problems. Numerical examples and fabrication test demonstrate that planar periodic frame structures exhibiting negative Poisson's ratio can be successfully obtained by the proposed method.

Keywords

Negative Poission's ratio; Auxetic structure; Topology optimization; Integer optimization; Local search.

1 Introduction

Poisson's ratio of isotropic bodies is constrained theoretically to the range $-1 \leq \nu \leq 1/2$ by thermodynamics. The majority of materials, however, are characterized by Poisson's ratio in the range $0 < \nu < 1/2$. Materials with negative Poisson's ratio will expand transversely when stretched longitudinally. Some naturally occurred materials, e.g., cadmium [20], single crystals of arsenic [15], and natural layered ceramics [36], exhibit negative Poisson's ratio. Extensive study of negative Poisson's ratio materials was initiated by the seminal work of Lakes [17], which developed polymer foams having this counter-intuitive property.

Materials with negative Poisson's ratio are also called *auxetic materials* [9]. We call structures exhibiting auxetic behavior *auxetic structures*. Auxetic property of materials usually stems from a particular geometrical structure, e.g., re-entrant structures [7, 11, 18, 40], chiral structures [14], multiscale laminates [27], rotating sub-structures [13], microporous foams [5], many-body systems with isotropic pair interactions [30], and porous elastomer with specific patterns [4]. Fabrics with

[†]Present address: Tokyo Keiki, Inc. 2-16-46, Minami-Kamata, Ohta, Tokyo 144-8551, Japan.

[‡]Corresponding author. Address: Department of Mathematical Informatics, Graduate School of Information Science and Technology, University of Tokyo, Tokyo 113-8656, Japan. E-mail: `kanno@mist.i.u-tokyo.ac.jp`. Phone: +81-3-5841-6906, Fax: +81-3-5841-6886.

auxetic property were also produced by using weft-knitting technology [22] and helical yarns [26, 35]. Scale of such geometrical structures of materials ranges from microscopic to naked-eye level. Every material has a structure in general, and, in this sense, distinction between materials and structures is obscure. This paper primarily concerns periodic structures, rather than materials, representative unit cells of which are visible with the naked eye; see numerical examples in section 5. However, when relatively small unit cell is repeated sufficiently many times, obtained periodic structures may approach to materials. Potential applications of auxetic materials and structures include tunable filters [2], artificial intervertebra discs [24], fasteners [6], and fibers for reinforcing composite materials [34]. See [1, 8, 12, 21, 28, 41] for more detailed surveys on auxetic materials.

A methodology of material design based on topology optimization of structures was proposed by Sigmund [33], where repetitive base unit of a material is modeled as a truss structure. The method was applied to find a material with prescribed negative Poisson's ratio. Topology optimization of continua based on the homogenization method was also applied to design microstructures with negative Poisson's ratio [3, 19, 32]. In [19], the obtained design of a planar periodic microstructure with negative Poisson's ratio was fabricated using silicon surface micromachining. However, optimal solutions obtained by this method have so-called *gray areas* and manual post-processing by an operator is required before manufacturing process. As clearly mentioned in [19], thickness of hinge regions of the obtained optimal solutions has a great influence of Poisson's ratio and stress distribution, but thickness and shapes of hinges were decided by perception of an engineer. In contrast, as detailed below, the method proposed in this paper does not generate hinges and gray areas, which makes the method free from perception of engineers. In [32], the obtained design of a three-dimensional microstructure was fabricated using a manufactured selective electron beam melting system. However, to guarantee ease of manufacture of optimal solutions, optimization was started from a given auxetic structure, which may limit solutions explored in the process of optimization. Indeed, the shape of the optimal solution obtained in [32] was not drastically different from the initial solution. Matsuoka *et al.* [25] proposed a genetic algorithm to design a periodic structure with negative Poisson's ratio. This method also requires post-processing of interpreting the obtained solution.

This paper proposes an optimization method to design a planar periodic frame structure that exhibits a negative Poisson's ratio property. Based on the conventional ground structure method, we consider a topology optimization problem of a frame structure. The optimized frame structure serves as the smallest unit of a periodic structure. Section of each beam element is supposed to be chosen from a set of some given candidates. The optimization problem is reformulated as a *mixed integer linear programming* (MILP) problem. This reformulation is achieved as a natural extension of MILP formulations of topology optimization of trusses with discrete member cross-sectional areas [29] and that of continua with binary design variables [38].

We solve a topology optimization problem of frame structures with discrete design variables. Local stress constraints are addressed precisely, i.e., bounds for axial force and two end moments are imposed only on present beam elements. Therefore, the optimal solution has neither hinges nor thin members. It is often that an optimized structure with negative Poisson's ratio has hinge regions, where negative Poisson's ratio stems from link-mechanisms and/or compliant mechanisms. Thickness of hinges of such a solution should be adjusted carefully before manufacturing process, because a structure with thin hinges can sustain only small forces while with thick hinges a structure may lose mechanisms from which negative Poisson's ratio accrues. In contrast, a solution without hinges and thin members but with optimized negative Poisson's ratio may have an advantage in manufacturability in the sense that no post-processing is required. From another perspective, optimized frame structures obtained by the proposed method may robust against fabrication errors. In this paper we fabricate the obtained optimal solution by applying photo-etching to a stainless plate and confirm its negative Poisson's ratio property; see section 5.1.

By virtue of MILP formulation, small-scale optimization problems can be solved globally with, e.g., the branch-and-bound method. Several software packages, e.g., CPLEX [16], are available for this purpose. However, it is difficult to solve large-scale problems globally from a viewpoint of computational cost. Large-scale problems are attacked by hierarchical optimization with a local search heuristics, in which MILP problems are solved sequentially. We begin with a coarse ground structure, for which the optimization problem is solved globally. The obtained optimal solution is then transferred to a refined ground structure, for which the optimization problem is solved locally with a local search. Specifically, the MILP problem is solved within a neighborhood of the current solution. The local search with MILP was suggested by Stolpe and Stidsen [37] to solve topology optimization of continua. The idea of using a coarser design domain to produce a good initial solution for a finer design domain was also proposed for topology optimization of continua in [37, 39].

The paper is organized as follows. In section 2 we present a concept of design problem of periodic frame structures with negative Poisson's ratio. In section 3 this design problem is formulated as an MILP problem. In section 4 we propose a hierarchical optimization method with local search heuristics to solve large-scale problems. In section 5 we demonstrate numerical experiments. An example of fabricated physical model is also presented. We conclude in section 6.

2 Design problem of auxetic structures

In this section we present a concept of design problem of an auxetic periodic structure which is realized by arranging a basic frame unit repeatedly. The frame unit is found by solving an optimization problem that will be formulated in section 3.

We consider a planar frame structure with the following properties:

(i) The structure has periodicity, as shown in Figure 1, where a unique base cell, i.e., the smallest unit, is connected repeatedly.

(ii) If the upper boundary is subjected to uniform displacement in the positive direction of the Y-axis in Figure 1, then displacement in the positive direction of the X-axis is induced on the right boundary, i.e., the structure exhibits negative Poisson's ratio behavior.

(iii) Negative Poisson's ratio property of the structure is invariant when roles of input and output boundaries in (ii) are swapped, i.e., the base cell has symmetric configuration.

Due to periodicity of the structure, our design domain is the base cell shown in Figure 2(a). Symmetry of the structure implies that configuration of the base cell is symmetric with respect to

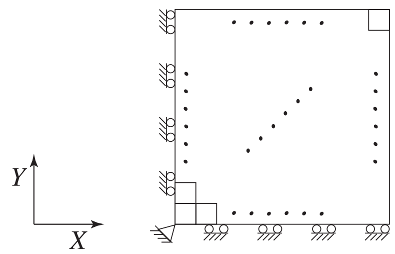

Figure 1: A planar periodic structure.

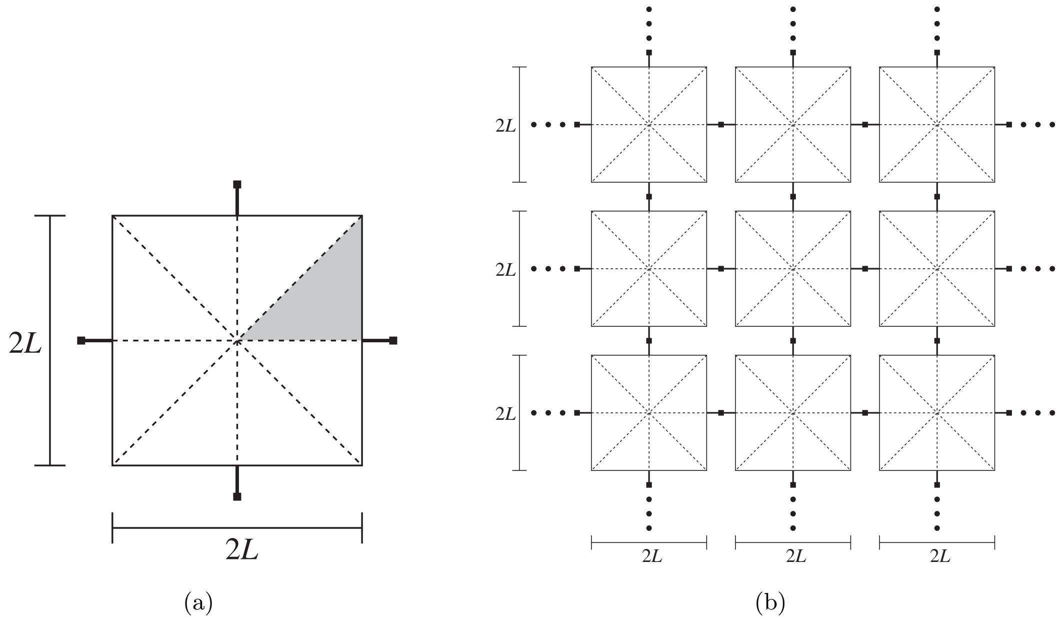

Figure 2: Schematic overview of a repeated planar frame structure. (a) Design domain of a base cell; and (b) a repeated frame structure obtained by connecting base cells.

reflection across the dashed lines. Therefore, an eighth of the base cell, shaded in Figure 2(a), is an independent design domain. The base cell has four outer short beams that serve as interfaces to an adjacent cell as shown in Figure 2(b).

Figure 3(a) shows an example of ground structure, which corresponds to a quarter of a base cell. The dashed line is an axis of symmetry of design. To obtain negative Poisson's ratio property, we consider the following design problem. The top-left node, called the *input node*, of the ground structure is subjected to a prescribed displacement, $\bar{u}_{\rm in} > 0$. Let $u_{\rm out}$ denote the displacement of the bottom-right node, called the *output node*. Then we solve a topology optimization problem that attempts to maximize $u_{\rm out}$, where beam sections are considered design variables. In this paper we call $-u_{\rm out}/u_{\rm in}$ Poisson's ratio of the structure.

Thus, we solve a topology optimization problem that maximizes the output displacement at the equilibrium state corresponding to the prescribed input displacement. This problem, however, has meaningless optimal solutions, because stiffness of the structure against external loads is not taken into account. As an extreme example, if all the members of the ground structure vanish, then the output node can move freely. Therefore, the null structure is (one of) optimal solutions, where the optimal value is positive infinity. Also, even if there are some existing members, the output node

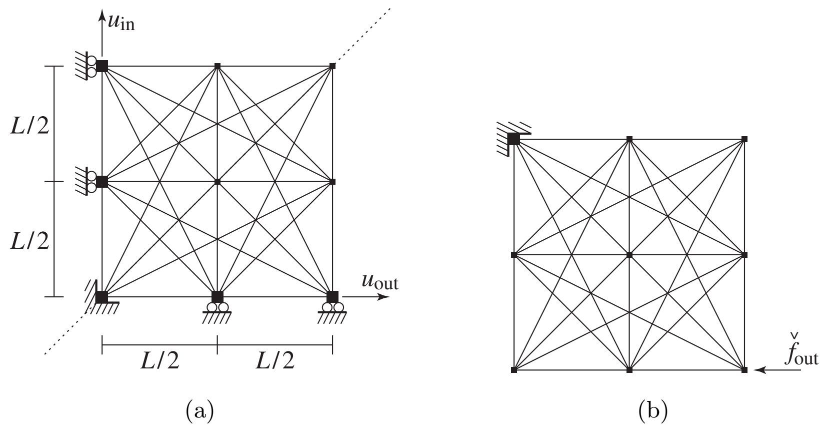

Figure 3: Problem setting with 2×2 grid ground structure. (a) The actual boundary condition corresponding to auxetic behavior; and (b) the fictitious boundary condition for the connectedness constraint.

can move freely if the members are not connected. To make the optimization problem meaningful, the feasible set is limited to connected structures. More precisely, topology of a structure should contain a connected path from the input node to the output node. To guarantee this condition, we consider a fictitious boundary condition shown in Figure 3(b) and require that the structure has an equilibrium state under this fictitious boundary condition. If such an equilibrium state exists, then there exists flow of internal forces from the output node (where the fictitious external load is applied) to the input node (where the fictitious reaction force acts). This means that there is a connected path, consisting of existing members, from the output node to the input node, and hence the output displacement is bounded when the input displacement is prescribed.

Descriptive summary of the design problem is given as follows.

- Topology optimization of planar frame structures is solved within the framework of the common ground structure method. Sections of beams are design variables to be optimized.
- We attempt to maximize the displacement of the output node, $u_{\rm out}$, at the equilibrium state where the displacement of the input node, $u_{\rm in}$, is prescribed; see Figure 3(a).
- Stress constraints of members are fully addressed.
- Existence of mutually intersecting members is not accepted.
- Design variables are considered discrete, i.e., section of each beam is chosen from a set of some given candidates.
- To avoid meaningless disconnected structures being optimal, we require that the structure has an equilibrium state with fictitious boundary conditions; see Figure 3(b).

In section 3 we formulate this optimization problem explicitly and reformulate it as an MILP problem.

3 Mixed integer linear programming approach

Section 2 has presented a concept of design problem of a periodic planar structure with negative Poisson's ratio. In section 3.1 we formulate this design problem as a topology optimization problem of frame structures. This topology optimization problem is reduced to an MILP problem in section 3.2.

3.1 Optimization problem

Consider a planar frame structure that serves as a ground structure in conventional topology optimization. The structure consists of sufficiently many members and locations of the nodes are specified. We use E to denote the set of members. Figure 3(a) shows an example consisting of 9 nodes and $|E| = 28$ members, where any two nodes are connected by a candidate member unless it does not create an overlapping member. We adopt the Timoshenko beam theory for modeling the members.

For member i ($i \in E$), let a_i and I_i denote the cross-sectional area and the moment of inertia, respectively, which are considered design variables. The vector of these design variables are written as $\boldsymbol{a} = (a_i \mid i \in E)$ and $\boldsymbol{I} = (I_i \mid i \in E)$.

We choose the section of each member from a given set of finitely many available sections. Let a pair of $\bar{a}_p$ and $\bar{I}_p$ represent an available section, where $\bar{a}_p$ is the cross-sectional area and $\bar{I}_p$ is the moment of inertia. We denote by $\{(\bar{a}_p, \bar{I}_p) \mid p \in P\}$ the set of available sections, where $|P|$ corresponds to the number of available sections. Member i either takes one of these available sections or vanishes. This condition is written as

$$(a_i, I_i) \in \{(0,0)\} \cup \{(\bar{a}_p, \bar{I}_p) \mid p \in P\}, \quad \forall i \in E.$$

Let $\boldsymbol{u} \in \mathbb{R}^d$ and $\boldsymbol{f} \in \mathbb{R}^d$ denote the displacement vector and the external force vector, respectively, where d is the number of degrees of freedom. At the input node, the displacement is prescribed and hence the induced reaction force is unknown; see Figure 3(a). Therefore, $\boldsymbol{u}$ and $\boldsymbol{f}$ can be partitioned as

$$\boldsymbol{u} = \begin{bmatrix} \bar{u}_{\mathrm{in}} \\ u_{\mathrm{out}} \\ \boldsymbol{u}_{\mathrm{free}} \end{bmatrix}, \quad \boldsymbol{f} = \begin{bmatrix} f_{\mathrm{in}} \\ 0 \\ \boldsymbol{0} \end{bmatrix}, \tag{1}$$

where $u_{\mathrm{out}} \in \mathbb{R}$, $\boldsymbol{u}_{\mathrm{free}} \in \mathbb{R}^{d-2}$, and $f_{\mathrm{in}} \in \mathbb{R}$ are unknown variables and $\bar{u}_{\mathrm{in}} > 0$ is a specified value. Let $K \in \mathbb{R}^{d \times d}$ denote the stiffness matrix, which is determined by $\boldsymbol{a}$ and $\boldsymbol{I}$. The displacement vector induced by the given input displacement is obtained as the solution of the static equilibrium equations

$$K(\boldsymbol{a}, \boldsymbol{I})\boldsymbol{u} = \boldsymbol{f}$$

in conjunction with the boundary condition in (1). Throughout the paper we assume that deformation of a structure is small and that members consist of a linear elastic material; geometrical nonlinearity and material nonlinearity are not considered.

We next introduce stress constraints. Let $m_i^{(1)}$ and $m_i^{(2)}$ denote the two end moments of member i. We use q_i to denote the axial force. Stress constraints for frame structures may possibly be formulated in some different forms. In this paper we deal with interaction between the axial force and the end moment by making use of a familiar piecewise linear yield condition. Specifically, for each $i \in E$, we consider the following constraints involving quite simple effect of interaction:

$$\frac{|q_i(\boldsymbol{u})|}{q_i^{\mathrm{y}}} + \frac{|m_i^{(e)}(\boldsymbol{u})|}{m_i^{\mathrm{y}}} \le 1, \quad e = 1, 2. \tag{2}$$

Here, q_i^{y} and m_i^{y} are upper bounds for absolute values of the axial force and the end moment, respectively. For instance, these values are given according to the yield force and the yield moment as

$$q_i^{\mathrm{y}} = \bar{\sigma} a_i, \quad m_i^{\mathrm{y}} = \bar{\sigma} z_i \tag{3}$$

with

$$\bar{\sigma} = \gamma \sigma^{\mathrm{y}},$$

where σ^{y} is the flow stress, z_i is the plastic section modulus, and $\gamma \in]0,1[$ is a specified safety factor. It should be clear that the stress constraint, (2), is imposed only on existing members. If member i vanishes in the course of optimization, then constraint (2) should be removed.

We next consider a constraint excluding disconnected structures. With reference to Figure 3(b), recall that this constraint is translated into the existence of an equilibrium state under a given fictitious boundary condition. Let $\check{\boldsymbol{f}} \in \mathbb{R}^{\check{d}}$ denote the fictitious external load vector, where $\check{d}$ is the number of degrees of freedom under the fictitious boundary condition. Without loss of generality, $\check{\boldsymbol{f}}$ is partitioned as

$$\check{\boldsymbol{f}} = \begin{bmatrix} \bar{f}_{\mathrm{out}} \\ \boldsymbol{0} \end{bmatrix},$$

where $\bar{f}_{\mathrm{out}} > 0$ is a specified fictitious force applied at the output node. Location and rotation of the input node are supposed to be fixed. Let $\check{\boldsymbol{s}}_i \in \mathbb{R}^3$ denote the natural generalized stress of member i. The components of $\check{\boldsymbol{s}}_i$ are the two end moments and the axial force. The force-balance equation can be written as

$$\sum_{i \in E} \check{H}_i \check{\boldsymbol{s}}_i = \check{\boldsymbol{f}}, \tag{4}$$

where $\check{H}_i \in \mathbb{R}^{\check{d} \times 3}$ $(\forall i \in E)$ are constant matrices. Note that matrix $(\check{H}_i \mid i \in E) \in \mathbb{R}^{\check{d} \times 3|E|}$ corresponds to the equilibrium matrix under the fictitious boundary condition. If member i vanishes in the course of optimization, then it cannot transmit forces, i.e., the condition

$$a_i = 0 \quad \Rightarrow \quad \check{\boldsymbol{s}}_i = \boldsymbol{0} \tag{5}$$

should be satisfied. We treat (4) and (5) as constraints of the optimization problem. Then, feasibility requires existence of a path of internal forces from the output node (at which the fictitious load is applied) to the input node (which is considered the fictitious support). Hence, meaningless solutions that are disconnected are excluded by these constraints.

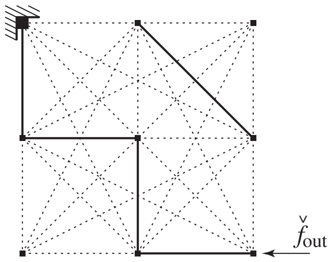

Figure 4: A solution satisfying (4) and (5).

Remark 3.1. Strictly speaking, constraints (4) and (5) do not exclude existence of floating members that are not irrelevant to a solution. An example is shown in Figure 4. In this case, a disconnected member can be ignored. A set of members that includes a path from the output node to the input node corresponds to an actual structure that we explore. ■

Presence of mutually intersecting members is avoided as follows. Let C denote the set of pairs of members that mutually intersect in the ground structure. Precisely, we write $(i, i') \in C$ if member i and member i' intersect. Then the two members cannot have positive cross-sectional areas simultaneously. Therefore, the constraint excluding intersecting members is formally written as

$$a_i a_{i'} = 0, \quad \forall (i, i') \in C. \tag{6}$$

By summing up the discussion above, the optimization problem for finding frame structures with negative Poisson's ratio is formulated as

$$\begin{aligned}
\max_{\boldsymbol{a}, \boldsymbol{I}, \boldsymbol{z}, \boldsymbol{u}, \check{\boldsymbol{s}}} \quad & u_{\mathrm{out}} && && \text{(7a)} \\
\mathrm{s.\,t.} \quad & K(\boldsymbol{a}, \boldsymbol{I})\boldsymbol{u} = \boldsymbol{f}, && && \text{(7b)} \\
& (f_{\mathrm{out}}, \boldsymbol{f}_{\mathrm{free}}) = (0, \boldsymbol{0}), && && \text{(7c)} \\
& u_{\mathrm{in}} = \bar{u}_{\mathrm{in}}, && && \text{(7d)} \\
& \frac{|q_i(\boldsymbol{u})|}{q^{\mathrm{y}}(a_i)} + \frac{|m_i^{(e)}(\boldsymbol{u})|}{m^{\mathrm{y}}(z_i)} \le 1 \ \Leftarrow \ a_i > 0, && e = 1, 2, \ \forall i \in E, && \text{(7e)} \\
& \sum_{i \in E} \check{H}_i \check{\boldsymbol{s}}_i = \check{\boldsymbol{f}}, && && \text{(7f)} \\
& \check{\boldsymbol{s}}_i = \boldsymbol{0} \ \Leftarrow \ a_i = 0, && \forall i \in E, && \text{(7g)} \\
& a_i a_{i'} = 0, && \forall (i, i') \in C, && \text{(7h)} \\
& (a_i, I_i, z_i) \in \{(0,0,0)\} \cup \{(\bar{a}_p, \bar{I}_p, \bar{z}_p) \mid p \in P\}, && \forall i \in E, && \text{(7i)}
\end{aligned}$$

In this problem, we choose the beam section of each member, represented by (a_i, I_i, z_i), according to (7i). Constraints (7b), (7c), and (7d) describe the equilibrium state, and hence auxetic property is achieved by maximizing u_{out}. In (7e), stress constraints are imposed only on existing members. Existence of $\check{\boldsymbol{s}}$ ($\forall i \in E$) satisfying (7f) and (7g) guarantees connectedness of members. Presence of mutually intersecting members is avoided by (7h).

In section 3.2 we reduce problem (7) to an MILP problem. A key idea for this reformulation is based on the MILP formulations for topology optimization of continua with 0–1 design variables [38]

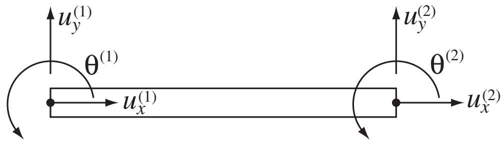

Figure 5: Local coordinate system for a beam element.

and of trusses with discrete member cross-sectional areas [29]. We extend this idea to topology optimization of frame structures.

3.2 Mixed integer linear programming reformulation

The design problem of a periodic frame structure with negative Poisson's ratio was formulated as an optimization problem, (7), in section 3.1. In this section, problem (7) is reduced to an MILP problem, which will be presented in (33).

For each $i \in E$, we introduce 0–1 variables, x_{ip} ($\forall p \in P$), to represent the section used for member i. We define $x_{ip} = 1$ if member i has section p, otherwise $x_{ip} = 0$. More precisely, x_{ip} ($\forall p \in P$) are subjected to the constraints

$$\sum_{p \in P} x_{ip} \le 1, \tag{8}$$

$$x_{ip} \in \{0, 1\}, \quad \forall p \in P. \tag{9}$$

Then the cross-sectional area, a_i, and the moment of inertia, I_i, of member i are expressed as

$$a_i = \sum_{p \in P} \bar{a}_p x_{ip}, \tag{10}$$

$$I_i = \sum_{p \in P} \bar{I}_p x_{ip}. \tag{11}$$

These conditions correspond to constraint (7i).

Constraints (7b) and (7e) are reformulated as follows. We begin by decomposing the stiffness matrix, $K(\boldsymbol{a}, \boldsymbol{I})$, in (7b). Consider the local coordinate system for member i as shown in Figure 5. The element displacement vector is written as $\boldsymbol{u}_i^{\mathrm{e}} = (u_x^{(1)}, u_y^{(1)}, \theta^{(1)}, u_x^{(2)}, u_y^{(2)}, \theta^{(2)})^\top$. The displacement vector of the ground structure, $\boldsymbol{u} \in \mathbb{R}^d$, is defined with respect to the global coordinate system. For each $i \in E$, transformation of $\boldsymbol{u}$ to $\boldsymbol{u}_i^{\mathrm{e}}$ is written as

$$\boldsymbol{u}_i^{\mathrm{e}} = T_i \boldsymbol{u},$$

where $T_i \in \mathbb{R}^{6 \times d}$ is a constant transformation matrix. We employ the Timoshenko beam theory to model the ground structure. Let $K_i^{\mathrm{e}}(a_i, I_i) \in \mathbb{R}^{6 \times 6}$ denote the member stiffness matrix defined with respect to the local coordinate system. Since K_i^{e} is a symmetric matrix and its rank is three, it can be written as

$$K_i^{\mathrm{e}}(a_i, I_i) = \sum_{j=1}^{3} k_{ij} \hat{\boldsymbol{b}}_{ij} \hat{\boldsymbol{b}}_{ij}^\top. \tag{12}$$

In (12), constant vectors $\hat{\boldsymbol{b}}_{i1}$, $\hat{\boldsymbol{b}}_{i2}$, $\hat{\boldsymbol{b}}_{i3} \in \mathbb{R}^3$ are defined by

$$\hat{\boldsymbol{b}}_{i1} = \begin{bmatrix} -1 \\ 0 \\ 0 \\ 1 \\ 0 \\ 0 \end{bmatrix}, \quad \hat{\boldsymbol{b}}_{i2} = \begin{bmatrix} 0 \\ -1 \\ -l_i/2 \\ 0 \\ 1 \\ -l_i/2 \end{bmatrix}, \quad \hat{\boldsymbol{b}}_{i3} = \begin{bmatrix} 0 \\ 0 \\ -1 \\ 0 \\ 0 \\ 1 \end{bmatrix}$$

and constants k_{i1}, k_{i2}, k_{i3} are defined by

$$k_{i1} = \frac{Ea_i}{l_i}, \tag{13a}$$

$$k_{i2} = \frac{1}{l_i}\Big(\frac{1}{\kappa G a_i} + \frac{l_i^2}{12EI_i}\Big)^{-1}, \tag{13b}$$

$$k_{i3} = \frac{EI_i}{l_i}. \tag{13c}$$

Here, E and G are Young's modulus and the shear modulus of the beam material, l_i is length of the beam element, and κ is the shear correction factor in the Timoshenko beam theory. Note that definition (13b) of k_{i2} is according to the MacNeal element of Timoshenko beam [23]. In our problem, beams are subjected to nodal loads only; intermediate loads and distributed loads are not applied. In this case, the MacNeal element coincides with the interdependent interpolation element [31], and hence the nodal displacement of a beam can be predicted exactly with single element [10, 31].

Let q_i and τ_i denote the axial and transverse shear forces, respectively. We denote by $m_i^{(1)}$ and $m_i^{(2)}$ the two end moments. The force-balance equation regarding member i is given by

$$\sum_{j=1}^{3} s_{ij}\hat{\boldsymbol{b}}_{ij} = \hat{\boldsymbol{f}}_i, \tag{14}$$

where $\hat{\boldsymbol{f}}_i = (-q_i, -\tau_i, m_i^{(1)}, q_i, \tau_i, m_i^{(2)})^\top$ is the nodal force vector and $\boldsymbol{s}_i = (s_{i1}, s_{i2}, s_{i3})^\top$ is the generalized stress vector. Physical interpretation of the components of $\boldsymbol{s}_i$ is obtained from (14) as

$$s_{i1} = q_i, \tag{15a}$$

$$s_{i2} = \tau_i = -\frac{m_i^{(1)} + m_i^{(2)}}{l_i}, \tag{15b}$$

$$s_{i3} = \frac{-m_i^{(1)} + m_i^{(2)}}{2}. \tag{15c}$$

By assembling member stiffness matrices in (12) in the usual way, the global stiffness matrix of the structure, denoted $K(\boldsymbol{a}, \boldsymbol{I}) \in \mathbb{R}^{d \times d}$, is obtained as

$$K(\boldsymbol{a}, \boldsymbol{I}) = \sum_{i \in E} \sum_{j=1}^{3} k_{ij}(a_i, I_i)\boldsymbol{b}_{ij}\boldsymbol{b}_{ij}^\top, \tag{16}$$

where constant vectors $\boldsymbol{b}_{i1}$, $\boldsymbol{b}_{i2}$, $\boldsymbol{b}_{i3} \in \mathbb{R}^d$ are defined by

$$\boldsymbol{b}_{ij} = T_i^\top \hat{\boldsymbol{b}}_{ij}, \quad j = 1, 2, 3.$$

By using expression (16), we decompose the global equilibrium equation, (7b). The global force-balance equation is written as

$$\sum_{i \in E} \sum_{j=1}^{3} s_{ij} \boldsymbol{b}_{ij} = \boldsymbol{f}. \tag{17}$$

where $\boldsymbol{s}_i$ is the generalized stress vector defined by (15). By introducing variables $\tilde{v}_{ij} \in \mathbb{R}$ $(j = 1, 2, 3)$ for each $i \in E$, $\boldsymbol{s}_i$ is related to $\boldsymbol{u}$ as

$$s_{ij} = k_{ij}(a_i, I_i) \tilde{v}_{ij}, \quad j = 1, 2, 3, \tag{18}$$

$$\tilde{v}_{ij} = \boldsymbol{b}_{ij}^\top \boldsymbol{u}, \quad j = 1, 2, 3, \tag{19}$$

Here, $\tilde{\boldsymbol{v}}_i = (\tilde{v}_{i1}, \tilde{v}_{i2}, \tilde{v}_{i3})^\top$ is a generalized strain vector conjugate to $\boldsymbol{s}_i$. Note that (18) and (19) correspond to the constitutive law and the compatibility relation, respectively. Certainly, by eliminating $\tilde{v}_{ij}$ and s_{ij}, (17), (18), and (19) revert to (7b). Expression (18), (19), and (17) is basis of our MILP formulation. We eliminate s_{ij}'s for convenience. Substitution of (18) into (15) and (17) read

$$k_{i1}(a_i, I_i) \tilde{v}_{i1} = q_i, \tag{20a}$$

$$k_{i2}(a_i, I_i) \tilde{v}_{i2} = -\frac{m_i^{(1)} + m_i^{(2)}}{l_i}, \tag{20b}$$

$$k_{i3}(a_i, I_i) \tilde{v}_{i3} = \frac{-m_i^{(1)} + m_i^{(2)}}{2}, \tag{20c}$$

and

$$\sum_{i \in E} \sum_{j=1}^{3} k_{ij}(a_i, I_i) \tilde{v}_{ij} \boldsymbol{b}_{ij} = \boldsymbol{f}. \tag{21}$$

For each $i \in E$, we introduce new variables $v_{ijp} \in \mathbb{R}$ $(j = 1, 2, 3;\ p \in P)$ as

$$v_{ijp} = \begin{cases} 0 & \text{if } x_{ip} = 0, \\ \tilde{v}_{ij} & \text{if } x_{ip} = 1, \end{cases} \quad \forall i, j, p. \tag{22}$$

Since $x_{ip} = 1$ implies that member i has section $(\bar{a}_p, \bar{I}_p)$, (21) can be rewritten as

$$\sum_{i \in E} \sum_{p \in P} \sum_{j=1}^{3} \bar{k}_{ijp} v_{ijp} \boldsymbol{b}_{ij} = \boldsymbol{f}, \tag{23}$$

where $\bar{k}_{ijp}$'s are constants defined by

$$\bar{k}_{ijp} = k_{ij}(\bar{a}_p, \bar{I}_p) \tag{24}$$

and the definition of k_{ij} was given by (13). On the other hand, condition (22) is equivalent to

$$\Big| \sum_{p \in P} v_{ijp} - \boldsymbol{b}_{ij}^\top \boldsymbol{u} \Big| \le M \Big(1 - \sum_{p \in P} x_{ip} \Big), \quad \forall i, j, \tag{25}$$

$$\sum_{j=1}^{3} |v_{ijp}| \le M x_{ip}, \quad \forall i, p, \tag{26}$$

where $M \gg 0$ is a sufficiently large constant.

Furthermore, condition (26) can be replaced with the stress constraints, (7e). Specifically, we next show that (7e) can be reformulated as

$$\frac{\bar{k}_{i1p}}{\bar{q}_p^{\mathrm{y}}}|v_{i1p}| + \frac{l_i}{2}\frac{\bar{k}_{i2p}}{\bar{m}_p^{\mathrm{y}}}|v_{i2p}| + \frac{\bar{k}_{i3p}}{\bar{m}_p^{\mathrm{y}}}|v_{i3p}| \leq x_{ip}, \quad \forall p \in P,\ \forall i \in E, \tag{27}$$

where $\bar{q}_p^{\mathrm{y}}$ and $\bar{m}_p^{\mathrm{y}}$ are positive constants defined below. Since all the constants in (27) are positive, (27) implies (26). In other words, (27) is a tighter constraint than (26). Recall that the stress constraints are formulated as (2). Observe that (2) is equivalent to

$$\frac{|q_i|}{q_i^{\mathrm{y}}} + \frac{1}{2}\frac{|m_i^{(1)} + m_i^{(2)}|}{m_i^{\mathrm{y}}} + \frac{1}{2}\frac{|m_i^{(1)} - m_i^{(2)}|}{m_i^{\mathrm{y}}} \leq 1. \tag{28}$$

Substitution of (15) into (28) yields

$$\frac{k_{i1}}{q_i^{\mathrm{y}}}|v_{i1}| + \frac{l_i}{2}\frac{k_{i2}}{m_i^{\mathrm{y}}}|v_{i2}| + \frac{k_{i3}}{m_i^{\mathrm{y}}}|v_{i3}| \leq 1. \tag{29}$$

In accordance with (3), define constants $\bar{q}_p^{\mathrm{y}}$ and $\bar{m}_p^{\mathrm{y}}$ by

$$\bar{q}_p^{\mathrm{y}} = \bar{\sigma}\bar{a}_p, \quad \bar{m}_p^{\mathrm{y}} = \bar{\sigma}\bar{z}_p \tag{30}$$

for each $p \in P$. From (22), (24), and (30), we can see that constraint (29) is expressed by (27).

The upshot of the discussion above is that constraints (7b) and (7e), together with constraint (7i), are equivalently rewritten as (23), (25), and (27) in conjunction with the constraints on x_{ip}'s, i.e., (8) and (9).

Constraint (7g) can also be treated with 0–1 variables x_{ip}'s. Since $a_i = 0$ is equivalent to $\sum_{p\in P} x_{ip} = 0$, (7g) can be rewritten as

$$\sum_{j=1}^{3} |\check{s}_{ij}| \leq M \sum_{j\in P} x_{ip}, \quad \forall i \in E, \tag{31}$$

where $M \gg 0$ is a sufficiently large constant. For simplicity of presentation, we rewrite constraint (7f) in the same format as (17). Let $\check{\boldsymbol{b}}_{ij} \in \mathbb{R}^{\check{d}}$ $(j = 1, 2, 3)$ denote column vectors of $\check{H}_i$. Then (7f) is rewritten as

$$\sum_{i\in E}\sum_{j=1}^{3} \check{s}_{ij}\check{\boldsymbol{b}}_{ij} = \check{\boldsymbol{f}}.$$

Note that $\check{\boldsymbol{b}}_{ij} \neq \boldsymbol{b}_{ij}$ in general because of the difference of boundary conditions.

Constraint (6), which excludes presence of mutually intersecting members, can be formulated in terms of x_{ip}'s as follows. Recall that $a_i > 0$ is equivalent to $\sum_{p\in P} x_{ip} = 1$ and $a_i = 0$ is equivalent to $\sum_{p\in P} x_{ip} = 0$. Therefore, constraint (6) means that $\sum_{p\in P} x_{ip}$ and $\sum_{p\in P} x_{i'p}$ should not be equal to one simultaneously. This condition is written as

$$\sum_{p\in P} (x_{ip} + x_{i'p}) \leq 1, \quad \forall (i, i') \in C. \tag{32}$$

We are now in position to present the full expression of an MILP problem that we solve. Constraint (7i) is expressed by (10) and (11) with the 0–1 variables, x_{ip} ($i \in E;\ p \in P$), satisfying (8). Constraints (7b) and (7e) can be rewritten as (23), (25), and (27). Constraints (7c), (7d), and (7f) are linear constraints. Constraint (7g) can be reduced to (31). Constraint (7h) is expressed as (32). As a consequence, problem (7) is reduced to the following MILP problem:

$$\max_{\boldsymbol{x},\boldsymbol{u},\boldsymbol{v},\check{\boldsymbol{s}},\boldsymbol{f}} \quad u_{\mathrm{out}} \tag{33a}$$

$$\text{s. t.} \quad \sum_{i \in E} \sum_{p \in P} \sum_{j=1}^{3} \bar{k}_{ijp} v_{ijp} \boldsymbol{b}_{ij} = \boldsymbol{f}, \tag{33b}$$

$$\Big| \sum_{p \in P} v_{ijp} - \boldsymbol{b}_{ij}^{\top} \boldsymbol{u} \Big| \le M \Big(1 - \sum_{p \in P} x_{ip} \Big), \quad \forall j = 1,2,3,\ \forall i \in E, \tag{33c}$$

$$(f_{\mathrm{out}}, \boldsymbol{f}_{\mathrm{free}}) = (0, \mathbf{0}), \tag{33d}$$

$$u_{\mathrm{in}} = \bar{u}_{\mathrm{in}}, \tag{33e}$$

$$\frac{\bar{k}_{i1p}}{\bar{q}_p^{\mathrm{y}}} |v_{i1p}| + \frac{l_i}{2} \frac{\bar{k}_{i2p}}{\bar{m}_p^{\mathrm{y}}} |v_{i2p}| + \frac{\bar{k}_{i3p}}{\bar{m}_p^{\mathrm{y}}} |v_{i3p}| \le x_{ip}, \quad \forall p \in P,\ \forall i \in E, \tag{33f}$$

$$\sum_{i \in E} \sum_{j=1}^{3} \check{s}_{ij} \check{\boldsymbol{b}}_{ij} = \check{\boldsymbol{f}}, \tag{33g}$$

$$\sum_{j=1}^{3} |\check{s}_{ij}| \le M \sum_{p \in P} x_{ip}, \quad \forall i \in E, \tag{33h}$$

$$\sum_{p \in P} (x_{ip} + x_{i'p}) \le 1, \quad \forall (i, i') \in C, \tag{33i}$$

$$\sum_{p \in P} x_{ip} \le 1, \quad \forall i \in E, \tag{33j}$$

$$x_{ip} \in \{0, 1\}, \quad \forall p \in P,\ \forall i \in E. \tag{33k}$$

In problem (33), continuous variables are $\boldsymbol{u}$, v_{ijp} ($\forall i, j, p$), $\check{s}_{ij}$ ($\forall i, j$), and $\boldsymbol{f}$, while 0–1 variables are x_{ip} ($\forall i, p$). All the constraints other than the integrality constraints, (33k), are linear constraints. Thus, problem (33k) is an MILP problem, and hence it can be solved globally with, e.g., a branch-and-cut algorithm. Several software packages, e.g., CPLEX [16], are available for this purpose.

Remark 3.2. As shown in Figure 2(a), we consider a base cell that has symmetry with respect to reflection across dashed lines, so that Poisson's ratio of the structure remains invariant when roles of the input and output nodes are exchanged. Because a ground structure corresponds to a quarter of the base cell, configuration of the optimized structure should have symmetry with respect to reflection across a dashed line in Figure 3(a). This symmetry condition is expressed as linear equality constraints in terms of x_{ip}'s as follows. Let S denote the set of pairs of members that are located at symmetric positions. In other words, we write $(i_1, i_2) \in S$ if member i_1 is swapped with member i_2 by reflection shown in Figure 3(a). If $(i_1, i_2) \in S$, then member i_1 and member i_2 should have same section. Hence, the symmetry constraint can be written as

$$x_{i_1 p} = x_{i_2 p}, \quad \forall p \in P,\ \forall (i_1, i_2) \in S.$$

This constraint is added to problem (33). ■

Remark 3.3. In the numerical examples presented in section 5, all members are supposed to have rectangular sections. In this particular case, constants in problem (33) are obtained concretely as follows. A rectangular section is characterized by its width $\bar{w}_p$ and thickness $\bar{t}_p$. The cross-sectional area, the plastic section modulus, and the moment of inertia are given by

$$\bar{a}_p = \bar{t}_p \bar{w}_p, \quad \bar{z}_p = \frac{1}{4}\bar{t}_p \bar{w}_p^2, \quad \bar{I}_p = \frac{1}{12}\bar{t}_p \bar{w}_p^3. \tag{34}$$

Then, $\bar{k}_{i1p}$, $\bar{k}_{i2p}$, and $\bar{k}_{i3p}$ in (33b) and (33f) are obtained from (13) and (24). Also, $\bar{q}_p^{\mathrm{y}}$ and $\bar{m}_p^{\mathrm{y}}$ in (33f) are obtained by substituting (34) into (30). ■

Remark 3.4. In the numerical examples in section 5 each member is determined either to have a specified section or to be removed, i.e., $|P| = 1$, although problem (33) allows more general cases that more than one candidate sections are given, i.e., $|P| \geq 2$. ■

Remark 3.5. Problem (33) includes a large constant, M, in (33c) and (33h). It is known that such a large constant, called "big-M," often slows down the solution process if it is chosen larger than necessary, because it weakens relaxation problems of an MILP problem. Unfortunately, it is not easy to guess the smallest value of M in problem (33) in advance. ■

Remark 3.6. The connectedness condition of the structure, (33g) and (33h), implies that there exists at least one member connected to the output node. Therefore, any feasible solution of problem (33) satisfies

$$\sum_{i \in E_{\mathrm{out}}} \sum_{p \in P} x_{ip} \geq 1,$$

where $E_{\mathrm{out}} \subseteq E$ is the set of members connected to the output node. We add this condition to problem (33) as a valid inequality constraint. ■

4 Hierarchical local search

In section 3 we have proposed to solve an MILP problem (33) by a deterministic algorithm with guaranteed global optimality. However, this method is practically executed only when the number of members of the ground structure, $|E|$, is small. For instance, as shown in section 5.1.2, CPLEX ver. 12.2 [16] requires more than half an hour to solve the problem with $|E| = 66$ members. It is thus very difficult to solve larger problems with guaranteed global optimality from a viewpoint of computational cost. This motivates us to propose a local search heuristics applicable to problems with large $|E|$.

Figure 6 schematically depicts the solution procedure. As shown in Figure 6(a), we begin with a ground structure with the small number of members. MILP problem (33) for this coarse ground structure is solved globally. Suppose that the optimal solution is the structure shown in Figure 6(b). We next prepare a finer ground structure by increasing members. Figure 6(c) shows an example, where each member of the ground structure in Figure 6(a) is divided into two members by adding new nodes. Moreover, the ground structure in Figure 6(c) has some newly added members, because any two nodes are connected by a member. As shown in Figure 6(d), we translate the optimal solution for the coarse ground structure to the current ground structure. This solution used as an initial point for the local search performed on the current ground structure. The idea of using a

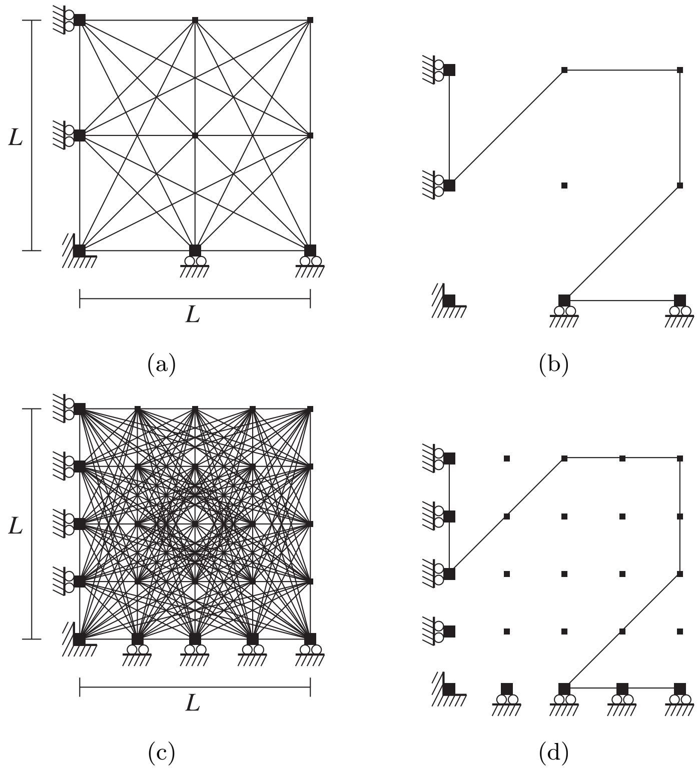

Figure 6: Overview of a hierarchical optimization approach. (a) A coarse ground structure; (b) the optimal solution for the coarse ground structure; (c) a refined ground structure; and (d) the initial solution for the refined ground structure.

coarser design domain to produce a good initial point for a finer design domain was originated with hierarchical optimization methods [37, 39] for topology optimization of continua.

We next describe the local search performed on a finer ground structure. The local search used here is essentially same as that in [37] and solves a sequence of MILP problems. Let $\boldsymbol{x}^*$ denote the current solution. For instance, $\boldsymbol{x}^*$ for the first iteration is the initial solution transfered from the optimal solution for a coarser ground structure; see Figure 6(d). We define a neighborhood of $\boldsymbol{x}^*$ with radius $r > 0$ by

$$N(\boldsymbol{x}^*, r) = \Big\{ \boldsymbol{x} \mid \sum_{i \in E} \sum_{p \in P} |x_{ip} - x_{ip}^*| \le r \Big\}.$$

The next solution is found from this neighborhood. Specifically, we solve MILP problem (33) with the constraint $\boldsymbol{x} \in N(\boldsymbol{x}^*, r)$, where r is fixed. Then the optimal value is no worse than the objective value at $\boldsymbol{x}^*$, because $\boldsymbol{x}^*$ is feasible. If the optimal value is improved, then we update the solution and repeat the local search. Otherwise, we terminate. As r decreases, the number of feasible solutions becomes smaller, and hence computational cost at each iteration might become smaller. On the other hand, with too small r the local search might possibly converge to a poor local optimal solution. This trade-off relation is common among most local search methods.

The hierarchical optimization with the local search is summarized as follows.

Algorithm 4.1.

Step 0: Choose a positive integer r and prepare the coarsest ground structure.

Step 1: Solve MILP problem (33). Let $\boldsymbol{x}^{\circ}$ denote the optimal solution.

Step 2: If the current ground structure is sufficiently fine, then declare $\boldsymbol{x}^{\circ}$ as the solution and terminate. Otherwise, refine the design domain with a finer ground structure and let $\boldsymbol{x}^{*}$ be representation of $\boldsymbol{x}^{\circ}$ on this new ground structure.

Step 3: Solve MILP problem (33) in conjunction with the constraint

$$\sum_{i \in E} \sum_{p \in P} |x_{ip} - x_{ip}^{*}| \le r. \tag{35}$$

Let $\boldsymbol{x}^{\circ}$ denote the optimal solution.

Step 4: If $\boldsymbol{x}^{\circ} = \boldsymbol{x}^{*}$, then go to step 2. Otherwise, let $\boldsymbol{x}^{*} := \boldsymbol{x}^{\circ}$ and go to step 3.

Note that constraint (35) can be expressed as some linear inequalities. Therefore, the problem solved at step 3 of this algorithm is also an MILP problem.

5 Numerical examples and fabrication

Auxetic structures are generated by solving MILP problem (33). Computation was carried out on two 2.66 GHz 6-Core Intel Xeon Westmere processors with 64 GB RAM. MILP problems were solved by using CPLEX ver. 12.2 [16]. The number of threads used by CPLEX was set as one. The other parameters are set as the default values.

In the following examples, all members have rectangular sections. Therefore, the shear correction factor of Timoshenko elements is $\kappa = 5/6$. In the ground structures of the examples, overlapping of members is avoided by removing the longer member when two members overlap. We suppose that only one beam section is available, i.e., $|P| = 1$, in each example. Section 5.1 collects relatively small problems which can be solved globally. In section 5.2 we solve larger problems with the hierarchical method presented in section 4.

5.1 Numerical experiments with single MILP problem

In this section we solve problems with relatively small numbers of design variables globally. In the examples of this section, Young's modulus and Poisson's ratio of the material are $E = 1\,\mathrm{GPa}$ and $\nu = 0.45$, respectively; the shear modulus of the material is given by $G = E/2(1+\nu)$. The upper bound for stress in (3) is $\bar{\sigma} = 2\,\mathrm{MPa}$.

5.1.1 Example (I)

Consider a ground structure shown in Figure 7(a). This structure consists of 9 nodes and $|E| = 28$ members. The side length of ground structures is $L = 12\,\mathrm{mm}$. The specified displacement at the input node is $\bar{u}_{\mathrm{in}} = 0.1\,\mathrm{mm}$. As for sections of beams, we consider two cases:

- Case (A): (width) $\times$ (thickness) $= 0.5\,\mathrm{mm} \times 0.5\,\mathrm{mm}$.

- Case (B): (width) $\times$ (thickness) $= 1.0\,\mathrm{mm} \times 0.25\,\mathrm{mm}$.

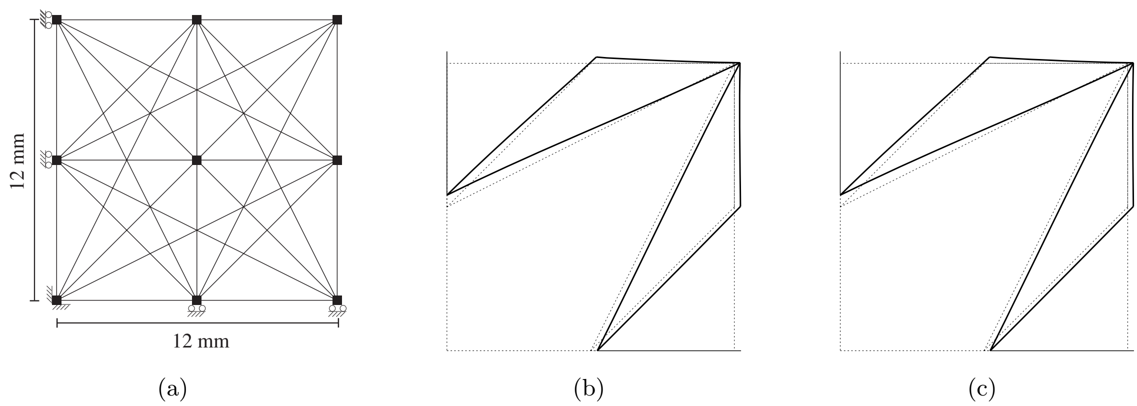

Figure 7: Example (I). (a) The ground structure; (b) the optimal solution in case (A); and (c) the optimal solution in case (B).

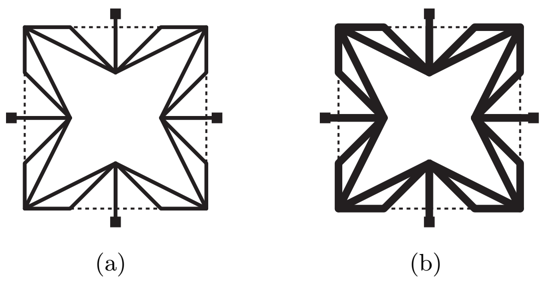

Figure 8: Optimal base cells of example (I): (a) Case (A); and (b) case (B).

Table 1: Computational results of example (I).

Beam section	$-u_{\mathrm{out}}/u_{\mathrm{in}}$	CPU (s)
(A)	-0.556608	1.38
(B)	-0.517468	0.72

The optimal solutions in case (A) and case (B) are shown in Figure 7(b) and Figure 7(c), respectively. In each figure, solid lines depict the deformed configuration with the prescribed input displacement, where the displacements are amplified five times. Computational results are listed in Table 1. Here, "CPU" means the computational time spent by CPLEX [16], and $-u_{\mathrm{out}}/u_{\mathrm{in}}$ corresponds to Poisson's ratio of the optimized structure.

Note that only a quarter of the base cell is analyzed in Figure 7. The entire shapes of the optimal base cells are shown in Figure 8.

5.1.2 Example (II)

We next consider a ground structure shown in Figure 9(a). This structure consists of 16 nodes and $|E| = 66$ members. The specified input displacement is $\bar{u}_{\mathrm{in}} = 0.12\,\mathrm{mm}$.

As for sections of beams, we consider two cases:

- Case (A): (width) $\times$ (thickness) $= 0.5\,\mathrm{mm} \times 0.5\,\mathrm{mm}$.

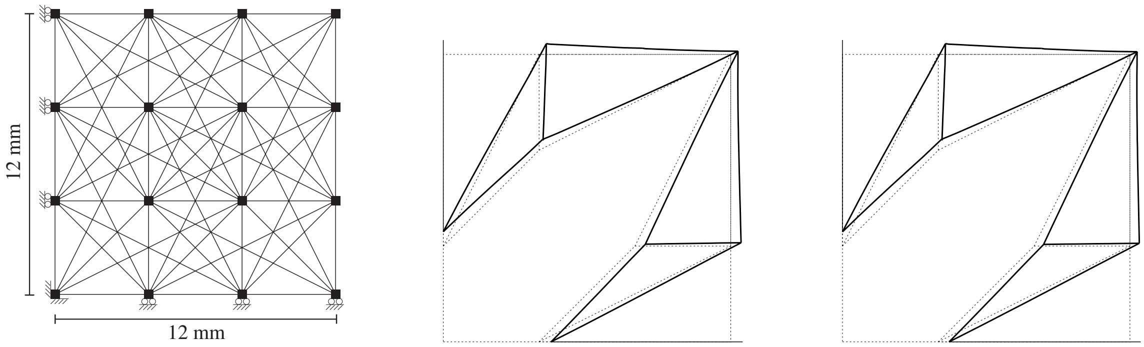

(a) (b) (c)

Figure 9: Example (II). (a) The ground structure; (b) the optimal solution in case (A); and (c) the optimal solution in case (B).

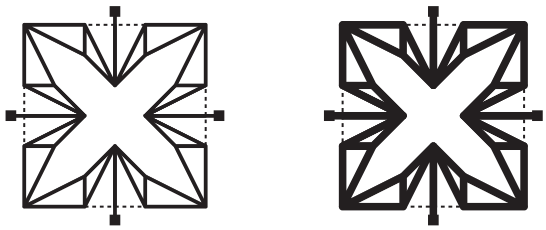

(a) (b)

Figure 10: Optimal base cells of example (II). (a) Case (A); and (b) case (B).

Table 2: Computational results of example (II).

Beam section	$-u_{\mathrm{out}}/u_{\mathrm{in}}$	CPU (s)
(A)	−0.832887	3,416.7
(B)	−0.752017	1,986.2

- Case (B): (width) × (thickness) = 1 mm × 0.25 mm.

The optimal solutions in case (A) and case (B) are shown in Figure 9(b) and Figure 9(c), respectively. The computational results are listed in Table 2. CPLEX [16] requires more than half an hour to solve an MILP problem. Figure 10 shows the optimized base cells, which are to be connected repeatedly to form auxetic periodic structures.

Roughly speaking, optimized base cells in section 5.1.1 and section 5.1.2 are approximately star-shaped, or octagons with re-entrant corners. Similar star-shaped auxetic structures have been known in literature; see, e.g., [17, 40].

5.1.3 Fabrication of structures

The optimal solution of section 5.1.2 was fabricated using photo-etching. A steel plate was coated by polyvinyl alcohol resist and then shape of the optimized base cell was exposed for masking.

The base cell in Figure 10 is repeated ten times twenty times as shown in Figure 11(a). Etching

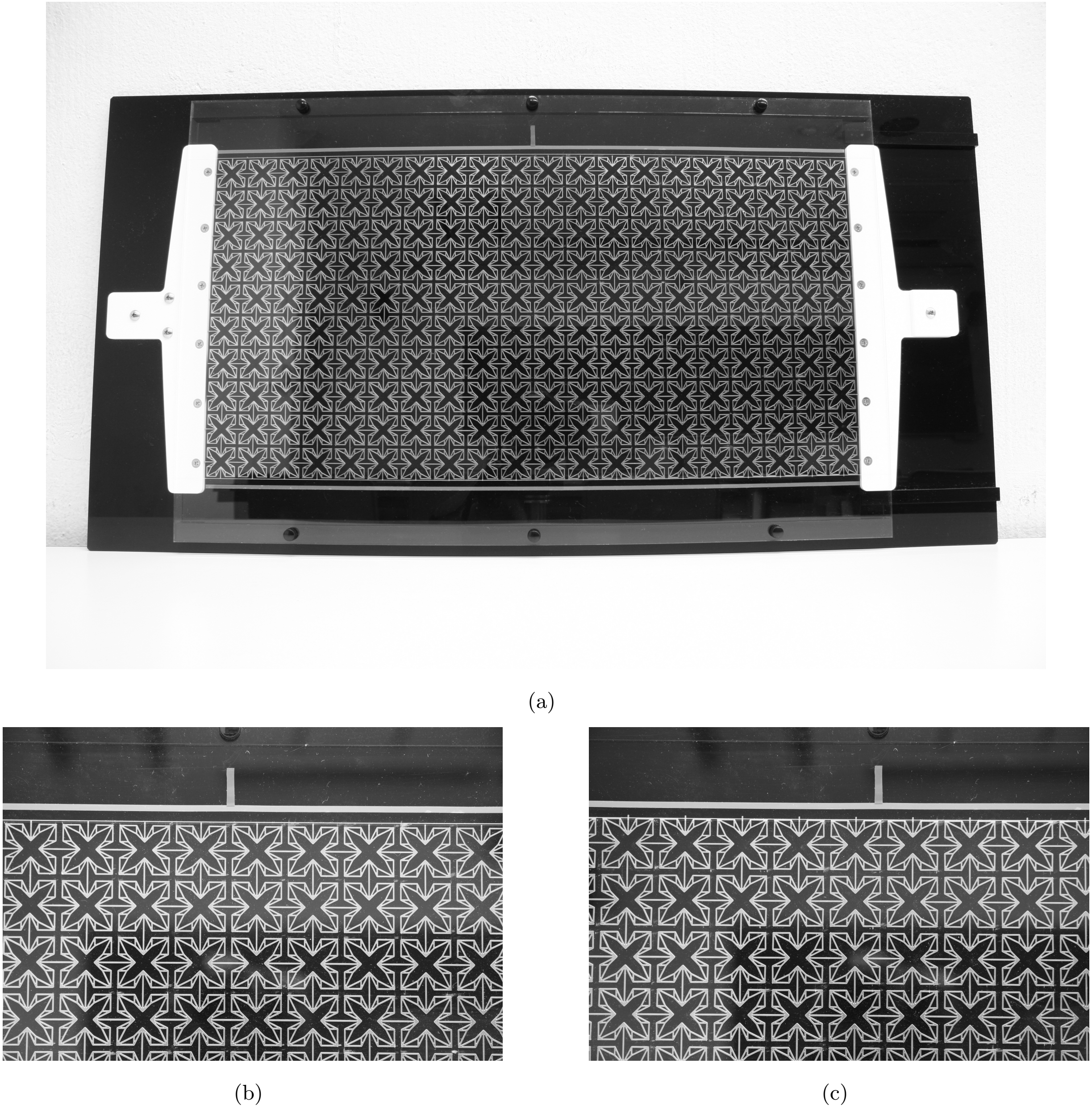

Figure 11: Fabricated optimal structure. (a) Testing structure composed of 20 by 10 base cells. The movable handle is seen on the right side and the handle on the left side is fixed; (b) undeformed configuration; and (c) deformed configuration.

was applied to stainless steel plate with thickness of 0.5 mm. The width of each beam is 0.75 mm. The left side of the structure in Figure 11(a) is fixed. The handle on the right side can be pulled a few millimeters in the right direction. Figure 11(b) shows a closeup view at the middle point of the upper side of the structure. The deformed configuration in Figure 11(c) shows that the structure expands vertically when it is stretched horizontally. Thus the structure has negative Poisson's ratio property.

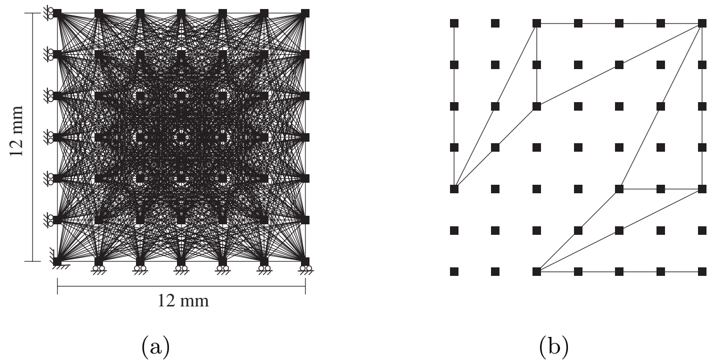

Figure 12: Example (III). (a) The ground structure; and (b) the initial solution.

Table 3: Computational results of example (III).

Iter.	$-u_{\mathrm{out}}/u_{\mathrm{in}}$	CPU (s)
0	-0.832887	—
1	-0.938312	22,609.4
2	-0.966160	7,248.3
3	-0.969188	6,569.2

5.2 Numerical experiments with hierarchical MILP method

In this section we attempt to solve problems involving many design variables by using the heuristics proposed in section 4.

5.2.1 Example (III)

Figure 12(a) shows a ground structure consisting of 49 nodes and $|E| = 748$ candidate members. For this problem, the ground structure of example (II), shown in Figure 9(a), serves as a coarser ground structure in hierarchical optimization. Accordingly, the optimal solution of example (II), shown in Figure 12(b), is adopted as the initial point from which the local search is started.

In this example, we use the following values: Young's modulus $E = 1\,\mathrm{GPa}$, material Poisson's ratio $\nu = 0.45$, beam width $0.5\,\mathrm{mm}$, beam thickness $0.5\,\mathrm{mm}$, input displacement $\bar{u}_{\mathrm{in}} = 0.1\,\mathrm{mm}$, and upper bound for stress $\bar{\sigma} = 3\,\mathrm{MPa}$. The size of neighborhood in (35) is $r = 4$. The objective value of the initial solution in Figure 12(b) is $-u_{\mathrm{out}}/u_{\mathrm{in}} = -0.832887$.

Algorithm 4.1 terminates after three iterations. Figure 13 shows convergence history of Algorithm 4.1 and Figure 14 shows the optimized base cell. Computational results are listed in Table 3.

5.2.2 Example (IV)

Figure 15(a) shows a ground structure consisting of 25 nodes and $|E| = 200$ candidate members. We regard the ground structure of example (I), shown in Figure 7(a), as a coarser ground structure for this problem. Accordingly, the optimal topology of example (I), shown in Figure 15(b), serves as the initial point from which the local search is started. In this example, we use the following values: Young's modulus $E = 70\,\mathrm{GPa}$, material Poisson's ratio $\nu = 0.45$, beam width $0.5\,\mathrm{mm}$, beam

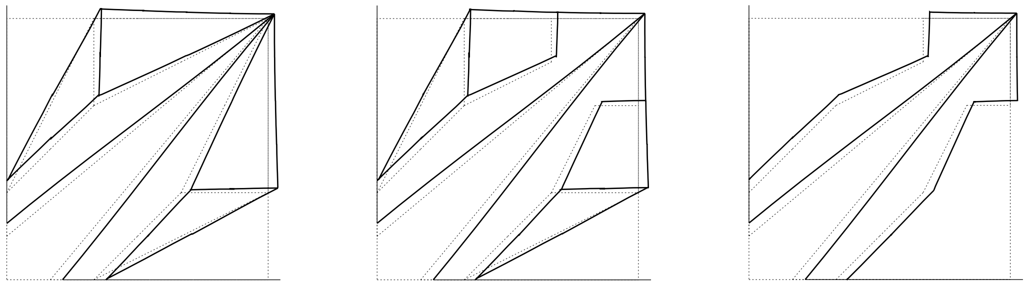

(a) (b) (c)

Figure 13: Convergence history of example (III). The solutions obtained at (a) the 1st iteration; (b) the 2nd iteration; and (c) the 3rd iteration.

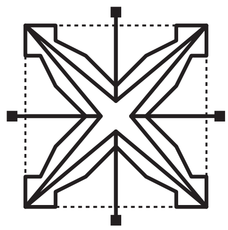

Figure 14: Obtained base cell of example (III).

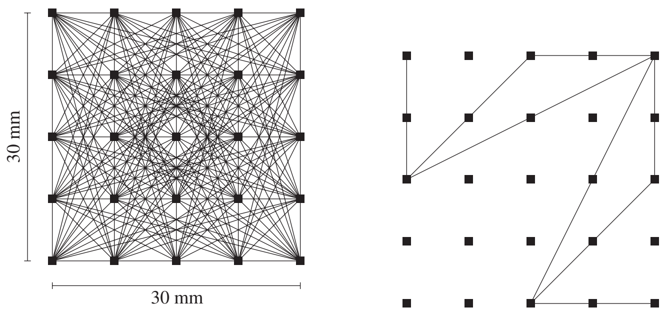

(a) (b)

Figure 15: Example (IV). (a) The ground structure; and (b) the initial solution.

thickness 0.5 mm, input displacement $\bar{u}_{\rm in} = 0.1$ mm, upper bound for stress $\bar{\sigma} = 50$ MPa. Since the ground structure has very thin members, the Euler–Bernoulli beam elements are usedin this example. The objective value of the initial solution in Figure 15(b) is $-u_{\rm out}/u_{\rm in} = -0.569530$.

As for size of neighborhood in (35), we consider four cases: $r = 4$, 6, 8, and 10. Computational results are listed in Table 4. Convergence histories of Algorithm 4.1 with $r = 4$, 6, 8, and 10 are illustrated in Figure 16, Figure 17, Figure 18, and Figure 19, respectively. Figure 20 shows the optimized base cells. Note that the same solution is obtained in the cases of $r = 4$ and $r = 8$. It is observed in Table 4 that computational cost of each iteration increases drastically as the size of neighborhood, r, increases. In contrast, the number of iterations for $r = 4$ is six and is larger than the other cases. When comparing the optimal values, the solution with $r = 6$ is slightly inferior to the solutions with $r = 4$ and $r = 8$. The solution with $r = 10$ is the best one, Poisson's ratio of which is very close to -1.

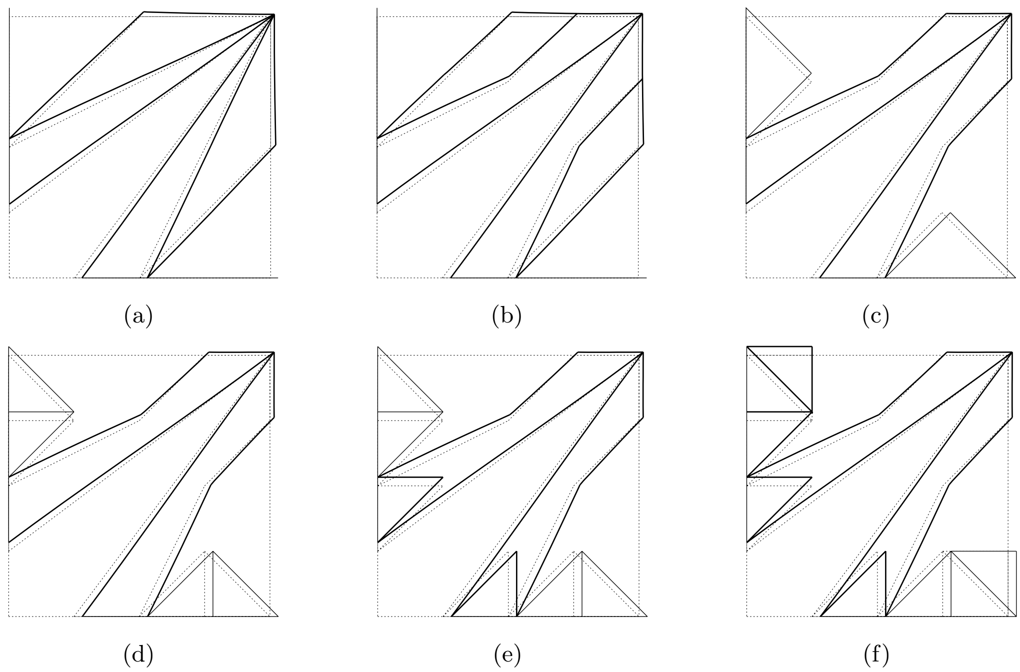

Figure 16: Convergence history of example (IV) with $r = 4$. The solutions obtained at (a) the 1st iteration; (b) the 2nd iteration; (c) the 3rd iteration; (d) the 4th iteration; (e) the 5th iteration; and (f) the 6th iteration.

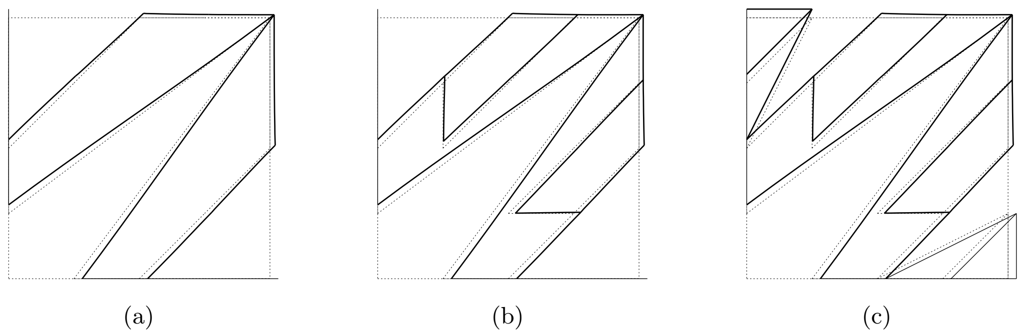

Figure 17: Convergence history of example (IV) with $r = 6$. The solutions obtained at (a) the 1st iteration; (b) the 2nd iteration; and (c) the 3rd iteration.

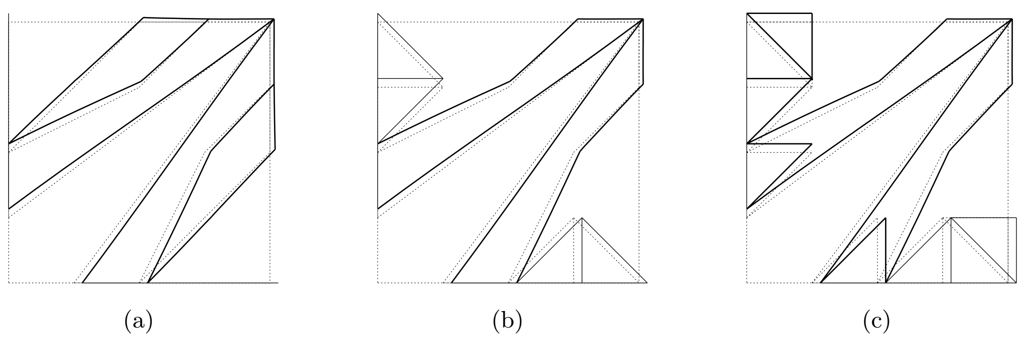

Figure 18: Convergence history of example (IV) with $r = 8$. The solutions obtained at (a) the 1st iteration; (b) the 2nd iteration; and (c) the 3rd iteration.

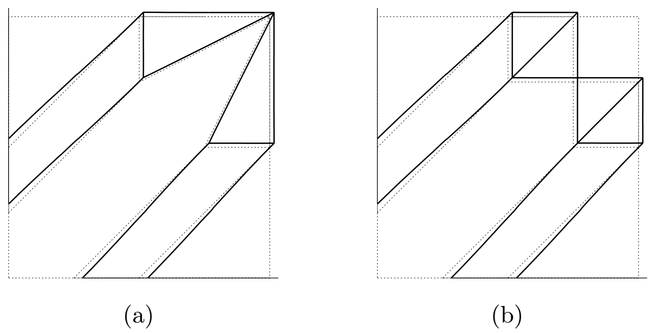

Figure 19: Convergence history of example (IV) with $r = 10$. The solutions obtained at (a) the 1st iteration; (b) the 2nd iteration; and (c) the 3rd iteration.

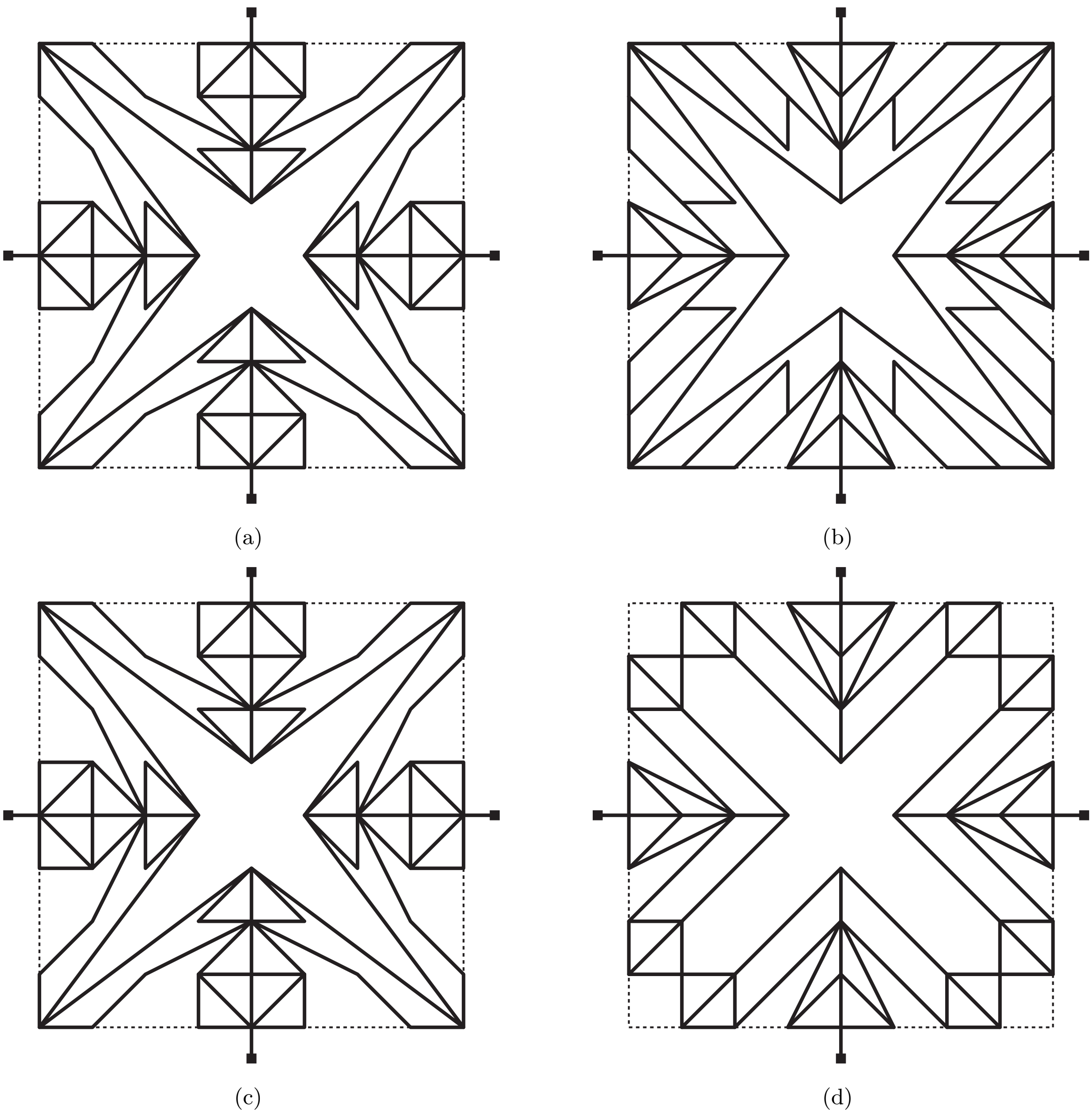

Figure 20: Obtained base cells of example (IV). (a) $r = 4$; (b) $r = 6$; (c) $r = 8$; and (d) $r = 10$.

Table 4: Computational results of example (IV).

Iter.	$r = 4$		$r = 6$		$r = 8$		$r = 10$	
	$-u_{\mathrm{out}}/u_{\mathrm{in}}$	CPU (s)	$-u_{\mathrm{out}}/u_{\mathrm{in}}$	CPU (s)	$-u_{\mathrm{out}}/u_{\mathrm{in}}$	CPU (s)	$-u_{\mathrm{out}}/u_{\mathrm{in}}$	CPU (s)
0	−0.569530	—	−0.569530	—	−0.569530	—	−0.569530	—
1	−0.856110	730	−0.953165	5,173	−0.954319	46,705	−0.982359	569,860
2	−0.954318	89	−0.955595	2,510	−0.955686	11,580	−0.983665	972,481
3	−0.955518	250	−0.955678	1,850	−0.955689	11,141	−0.983847	171,013
4	−0.955686	170						
5	−0.955689	289						
6	−0.955689	257						

6 Conclusions

Materials and structures with negative Poisson's ratio have been received significant interest for long years because of potential in various applications. This paper has explored possibility to design periodic frame structures that exhibit negative Poisson's ratio. Since local stress constraints are fully addressed and beam sections are chosen from given finitely many candidates, the obtained structure involves no link-mechanism. This is in contrast to continuum topology optimization approaches to gain negative Poisson's ratio, because optimal solutions obtained by those approaches usually involve link-mechanisms and/or compliant mechanisms [19, 32] and post-processing might be required if stress concentration is required to be avoided from the optimal solutions. Large-scale problems were solved with a local search heuristics, which is based on the mixed integer linear programming (MILP) formulation of the topology optimization problem. Numerical examples and a fabricated physical model have demonstrated that periodic frame structures exhibiting negative Poisson's ratio can be obtained by using the proposed method. Also, Poisson's ratios of the obtained solutions are almost equal to -1.

This paper has developed a generic framework for optimizing frame structures with discrete design variables of beam sections. Optimization concerning other structural performances can be formulated similarly, although computational efficiency should be examined. Regarding negative Poisson's ratio property, this paper has addressed only the ratio of the horizontal output displacement to the vertical input displacement. Effective Poisson's ratio of frames has not been considered. Also, issues of geometrical nonlinearity, as well as out-of-plane deformations, have not been addressed in this paper. Extension to three-dimensional structures remains to be studied. In this paper only simple square lattice-like connection of base cell has been studied. Other connectivity of base cell may possibly improve negative Poisson's ratio.

Acknowledgments

The work of the second author is partially supported by Grant-in-Aid for Scientific Research (C) 23560663 and by the Aihara Project, the FIRST program from JSPS, initiated by CSTP.

References

[1] Alderson, A.: A triumph of lateral thought. *Chemistry and Industry*, **17**, 384–391 (1999).

[2] Alderson, A., Rasburn, J., Ameer-Beg, S., Mullarkey, P.G., Perrie, W., Evans, K.E.: An auxetic filter: a tuneable filter displaying enhanced size selectivity or defouling properties. *Industrial and Engineering Chemistry Research*, **39**, 654–665 (2000).

[3] Bendsøe, M.P., Sigmund, O.: *Topology Optimization (2nd ed.)*. Springer-Verlag, Berlin (2003).

[4] Bertoldi, K., Reis, P.M., Willshaw, S., Mullin, T.: Negative Poisson's ratio behavior induced by an elastic instability. *Advanced Materials*, **22**, 361–366 (2010).

[5] Caddock, B.D., Evans, K.E.: Microporous materials with negative Poisson's ratios: I. Microstructure and mechanical properties. *Journal of Physics D: Applied Physics*, **22**, 1877–2882 (1989).

[6] Choi, J.B., Lakes, R.S.: Design of a fastener based on negative Poisson's ratio foam. *Cellular Polymers*, **10**, 205–212 (1991).

[7] Evans, K.E., Alderson, A., Christian, F.R.: Auxetic two-dimensional polymer networks. An example of tailoring geometry for specific mechanical properties. *Journal of the Chemical Society, Faraday Transactions*, **91**, 2671–2680 (1995).

[8] Evans, K.E., Alderson, K.L.: Auxetic materials: the positive side of being negative. *Engineering Science and Education Journal*, **9**, 148–154 (2000).

[9] Evans, K.E., Hutchinson, I.J., Rogers, S.C.: Molecular network design. *Nature*, **353**, 124 (1991).

[10] Friedman, Z., Kosmatka, B.: An improved two-node Timoshenko beam finite element. *Computers and Structures*, **47**, 473–481 (1993).

[11] Friis, E.A., Lakes, R.S., Park, J.B.: Negative Poisson's ratio polymeric and metallic foams. *Journal of Materials Science*, **23**, 4406–4414 (1988).

[12] Greaves, G.N., Greer, A.L., Lakes, R.S., Rouxel, T.: Poisson's ratio and modern materials. *Nature Materials*, **10**, 823–837 (2011).

[13] Grima, J.N., Alderson, A., Evans, K.E.: Auxetic behaviour from rotating rigid units. *Physica Status Solidi (b)*, **242**, 561–575 (2005).

[14] Grima, J.N., Gatt, R., Farrugia, P.: On the properties of auxetic meta-tetrachiral structures. *Physica Status Solidi (b)*, **245**, 511–520 (2008).

[15] Gunton, D.J., Saunders, G.A.: The Young's modulus and Poisson's ratio of arsenic, antimony and bismuth. *Journal of Materials Science*, **7**, 1061–1068 (1972).

[16] IBM ILOG: *User's Manual for CPLEX*. `http://www.ilog.com/` (2010).

[17] Lakes, R.: Foam structures with a negative Poisson's ratio. *Science*, **235**, 1038–1040 (1987).

[18] Lakes, R.: Deformation mechanisms in negative Poisson's ratio materials: structural aspects. *Journal of Materials Science*, **26**, 2287–2292 (1991).

[19] Larsen, U.D., Sigmund, O., Bouwstra, S.: Design and fabrication of compliant micromechanisms and structures with negative Poisson's ratio. *Journal of Microelectromechanical Systems*, **6**, 99–106 (1997).

[20] Li, Y.: The anisotropic behavior of Poisson's ratio, Young's modulus, and shear modulus in hexagonal materials. *Physica Status Solidi (a)*, **38**, 171–175 (1976).

[21] Liu, Y., Hu, H.: A review on auxetic structures and polymeric materials. *Scientific Research and Essays*, **5**, 1052–1063 (2010).

[22] Liu, Y., Hu, H., Lam, J.K.C., Liu, S.: Negative Poisson's ratio weft-knitted fabrics. *Textile Research Journal*, **80**, 856–863 (2010).

[23] MacNeal, R.H.: A simple quadrilateral shell element. *Computers and Structures*, **8**, 175–183 (1978).

[24] Martz, E.O., Lakes, R.S., Goel, V.K., Park, J.B.: Design of an artificial intervertebral disc exhibiting a negative Poisson's ratio. *Cellular Polymers*, **24**, 127–138 (2005).

[25] Matsuoka, T., Yamamoto, S., Takahara, M.: Prediction of structures and mechanical properties of composites using a genetic algorithm and finite element method. *Journal of Materials Science*, **36**, 27–33 (2001).

[26] Miller, W., Hook, P.B., Smith, C.W., Wang, X., Evans, K.E.: The manufacture and characterisation of a novel, low modulus, negative Poisson's ratio composite. *Composites Science and Technology*, **69**, 651–655 (2009).

[27] Milton, G.W.: Composite materials with Poisson's ratios close to -1. *Journal of the Mechanics and Physics of Solids*, **40**, 1105–1137 (1992).

[28] Prawoto, Y.: Seeing auxetic materials from the mechanics point of view: a structural review on the negative Poisson's ratio. *Computational Materials Science*, **58**, 140–153 (2012).

[29] Rasmussen, M.H., Stolpe, M.: Global optimization of discrete truss topology design problems using a parallel cut-and-branch method. *Computers and Structures*, **86**, 1527–1538 (2008).

[30] Rechtsman, M.C., Stillinger, F.H., Torquato, S.: Negative Poisson's ratio materials via isotropic interactions. *Physical Review Letters*, **101**, 085501 (2008).

[31] Reddy, J.N.: On locking-free shear deformable beam finite elements. *Computer Methods in Applied Mechanics and Engineering*, **149**, 113–132 (1997).

[32] Schwerdtfeger, J., Wein, F., Leugering, G., Singer, R.F., Körner, C., Stingl, M., Schury, F.: Design of auxetic structures via mathematical optimization. *Advanced Materials*, **23**, 2650–2654 (2011).

[33] Sigmund, O.: Materials with prescribed constitutive parameters: an inverse homogenization problem. *International Journal of Solids and Structures*, **31**, 2313–2329 (1994).

[34] Simkins, V.R., Alderson, A., Davies, P.J., Alderson, K.L.: Single fibre pullout tests on auxetic polymeric fibres. *Journal of Materials Science*, **40**, 4355–4364 (2005).

[35] Sloan, M.R., Wright, J.R., Evans, K.E.: The helical auxetic yarn—a novel structure for composites and textiles; geometry, manufacture and mechanical properties. *Mechanics of Materials* **43**, 476–486 (2011).

[36] Song, F., Zhou, J., Xu, X., Xu, Y., Bai, Y.: Effect of a negative Poisson ratio in the tension of ceramics. *Physical Review Letters*, **100**, 245502 (2008).

[37] Stolpe, M., Stidsen, T.: A hierarchical method for discrete structural topology design problems with local stress and displacement constraints. *International Journal for Numerical Methods in Engineering*, **69**, 1060–1084 (2007).

[38] Stolpe, M., Svanberg, K.: Modelling topology optimization problems as linear mixed 0–1 programs. *International Journal for Numerical Methods in Engineering*, **57**, 723–739 (2003).

[39] Svanberg, K., Werme, M.: Sequential integer programming methods for stress constrained topology optimization. *Structural and Multidisciplinary Optimization*, **34**, 277–299 (2007).

[40] Theocaris, P.S., Stavroulakis, G.E., Panagiotopoulos, P.D.: Negative Poisson's ratios in composites with star-shaped inclusions: a numerical homogenization approach. *Archive of Applied Mechanics*, **67**, 274–286 (1997).

[41] Yang, W., Li, Z.-M., Shi, W., Xie, B.-H., Yang, M.-B.: Review on auxetic materials. *Journal of Materials Science*, **39**, 3269–3279 (2004).